The Astrophysical Journal, 642:L41–L44, 2006 May 1


# ON KINEMATIC SUBSTRUCTURE IN THE SEXTANS DWARF SPHEROIDAL GALAXY[1]

Matthew G. Walker,[2] Mario Mateo,[2] Edward W. Olszewski,[3] Jayanta Kumar Pal,[4]
Bodhisattva Sen,[4] and Michael Woodroofe[4]

*Received 2006 March 1; accepted 2006 March 24; published 2006 April 14*

## ABSTRACT

We present multifiber echelle radial velocity results for 551 stars in the Sextans dwarf spheroidal galaxy and identify 294 stars as probable Sextans members. The projected velocity dispersion profile of the binned data remains flat to a maximum angular radius of 30′. We introduce a nonparametric technique for estimating the projected velocity dispersion surface and use this to search for kinematic substructure. Our data do not confirm previous reports of a kinematically distinct stellar population at the Sextans center. Instead we detect a region near the Sextans core radius that is kinematically colder than the overall Sextans sample with 95% confidence.

*Subject headings:* galaxies: dwarf — galaxies: individual (Sextans) — galaxies: kinematics and dynamics — Local Group

## 1. INTRODUCTION, OBSERVATIONS, AND DATA

The most recent kinematic studies of dwarf spheroidal galaxies (dSph's) show that radial velocity (RV) dispersion profiles of these dark matter–dominated systems are generally flat, with some evidence for a declining dispersion at large radius in Draco and Ursa Minor (Wilkinson et al. 2004; but see Muñoz et al. 2005; Walker et al. 2006; M. Mateo et al. 2006, in preparation). However, localized regions having enhanced stellar density or comparatively "cold" kinematics have been detected in some dSph's (Olszewski & Aaronson 1985; Kleyna et al. 2003, 2004; Coleman et al. 2004, 2005). Such substructure may be related to the star formation history of individual systems (Tolstoy et al. 2004; Olszewski et al. 2006) or may hint at a merger history (Coleman et al. 2004; Wilkinson et al. 2005). The presence of substructure in these tiny galaxies has cosmological implications as well. Kleyna et al. (2003) demonstrated that the apparent substructure in Ursa Minor should quickly disperse in the presence of a centrally cusped dark matter halo but can remain intact for a Hubble time in the potential of a cored halo. This raises doubts about whether the smallest galaxies conform to the universal density profile that results from simulations of cold dark matter (Navarro et al. 1997).

Here we present first results from an ongoing survey of dSph stellar RVs. We used the Michigan-MIKE Fiber System (MMFS) at the 6.5 m Magellan Clay Telescope at Las Campanas Observatory, in 2004 March and 2005 February, to obtain spectra of target stars selected from *VI* photometry of the Sextans red giant branch. A complete description of MMFS is forthcoming (M. G. Walker et al. 2006, in preparation). Briefly, 256 fibers placed over a field of diameter 30′ feed the two channels of the MIKE echelle spectrograph (Bernstein et al. 2003). Order-blocking filters isolate the 5140–5180 Å spectral region, which contains strong Mg I triplet absorption features and is free of the sky emission lines that contaminate the infrared Ca triplet. After binning, the spectra have resolution $R \sim 20{,}000$ (blue channel) and $R \sim 15{,}000$ (red channel).

The data reduction procedure is similar to that described in M. Mateo et al. (2006, in preparation). Briefly, after extracting and calibrating spectra, we measure RV using the IRAF task FXCOR, cross-correlating the spectrum of each target star against that of a high signal-to-noise ratio template composed of co-added spectra of RV standard stars. A series of quality controls yields a data set containing 810 RV measurements for 551 Sextans candidate members. We use multiple measurements of 173 stars from 12 partially overlapping fields to estimate measurement uncertainties as in Walker et al. (2006). The mean 1 $\sigma$ RV uncertainty is $\pm 2.6$ km s$^{-1}$.

Figure 1 plots the measured heliocentric RV versus angular distance from the Sextans center. The broad distribution of RV outliers away from the main peak at 226 km s$^{-1}$ is consistent with the RV distribution of foreground Milky Way dwarfs (whose magnitudes and colors place them inside our Sextans RGB selection region) predicted by the Besançon Milky Way model (Robin et al. 2003).[5] To determine membership, we use a biweight estimator (Beers et al. 1990) of distribution center and variance and iteratively reject RVs that lie more than 3 $\sigma$ from the distribution center. This algorithm yields a default sample of 294 probable Sextans members. Because the conventional 3 $\sigma$ cutoff is somewhat arbitrary, we repeat our analyses for possible samples containing 276 stars (2.6 $\sigma$ outlier rejection) and 303 stars (4 $\sigma$).

## 2. RV DISPERSION: PROFILE AND SURFACE

Figure 2 maps the projected positions of the likely Sextans members and indicates the magnitude of each star's RV relative to the sample mean. We detect no rotation—the maximum rotation signal of 0.9 km s$^{-1}$ is exceeded in 43% of Monte Carlo trials. Following the procedure described in Walker et al. (2006), we estimate from the default $N = 294$ sample a mean RV of $225.8 \pm 0.5$ km s$^{-1}$ and RV dispersion $8.9 \pm 0.4$ km s$^{-1}$, in agreement with Kleyna et al. (2004, hereafter K04). For $N = 276$ and $N = 303$ samples, the RV dispersions are $7.1 \pm 0.3$ and $10.3 \pm 0.5$ km s$^{-1}$, respectively. Binning by radius, we estimate the projected RV dispersion profile, $\sigma_p(R)$, using the Gaussian maximum likelihood method of K04 (see their eq. [1]). The RV dispersion calculated for a given bin is not affected if we modify K04's equation (1) to include a fractional component of Galactic contaminants with plausible (e.g., uniform within the accepted range) RV distribution.

[1] Based on observations using the Magellan telescopes.

[2] Department of Astronomy, University of Michigan, 830 Dennison Building, Ann Arbor, MI 48109-1042.

[3] Steward Observatory, University of Arizona, 933 North Cherry Avenue, Tucson, AZ 85721-0065.

[4] Department of Statistics, University of Michigan, 439 West Hall, Ann Arbor, MI 48109-1107.

[5] See http://bison.obs-besancon.fr/modele.

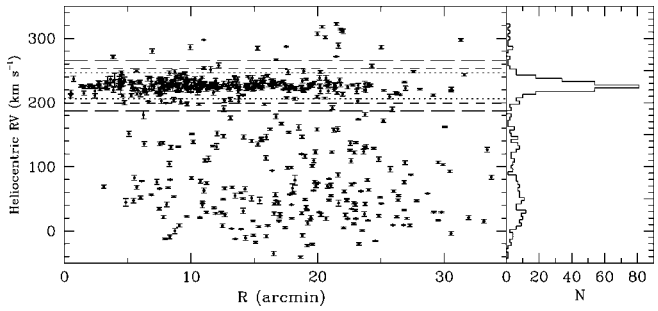


FIG. 1.—*Left*: Heliocentric RV vs. angular distance from the Sextans center ($\alpha = 10^h13^m03^s$, $\delta = -01°36'54''$, J2000; Mateo 1998). Dotted, short-dashed, and long-dashed lines mark boundaries of $N = 276$, $N = 294$, and $N = 303$ member samples, respectively. Not shown are 21 observed stars at $60' \leq R \leq 80'$, none of which are likely members. *Right*: Histogram of the Sextans RV distribution.

Figure 3 plots the Sextans RV dispersion profile calculated using a variety of bin sizes. Aside from setting the global RV dispersion value, choice of membership sample has little effect on the measured profile. As in K04, the top panels of Figure 3 use bins having regularly spaced outer boundaries at 5′, 10′, …, 30′. Our data do not reach the largest radii sampled by the K04 data, so we can neither confirm nor rule out the falling dispersion K04 detect at $R \geq 30'$. For $R < 30'$, our data indicate a flat Sextans profile. In contrast, K04 measured $\sigma_p \leq 1$ km s$^{-1}$ for the seven stars in their sample at $R < 5'$ (see Fig. 4 of K04). The 40 stars from our sample that occupy this region have $\sigma_p = 8.3^{+1.4}_{-0.8}$ km s$^{-1}$. The profiles shown in Figures 3*b* and 3*c* have annuli chosen such that bins contain equal numbers of stars. A "cold" inner profile point begins to emerge as the number of bins increases, but at the cost of diminished statistical significance. The profiles in Figure 3*c* use 43 bins (six stars per bin), the smallest number for which we find any annulus with $\sigma_p \leq 1$ km s$^{-1}$. Monte Carlo simulations indicate that one expects to measure such a small dispersion in about one of 43 bins even if the true profile is perfectly flat.[6]

We conclude that our data are consistent with a flat Sextans RV dispersion profile for $R < 30'$. This result is consistent with K04 if one omits their innermost point, as K04 do when using their observed profile to estimate a Sextans mass of $M(r \leq 1 \text{ kpc}) \sim 10^7$–$10^8\ M_\odot$. We require a more radially extended data set in order to further constrain the Sextans mass.

Our data set consists of measurements $\{(X_1, Y_1, V_1, \sigma_1), \ldots, (X_N, Y_N, V_N, \sigma_N)\}$, where $X_i$ and $Y_i$ give the projected position of the *i*th member star with respect to the Sextans center and $V_i$ and $\sigma_i$ are the measured RV and its formal uncertainty. To identify potential kinematic substructure, we search for regional anomalies in the RV distribution as a function of projected position. From the data we estimate the Sextans RV dispersion *surface* using a nonparametric Nadaraya-Watson estimator:

$$\widehat{\langle v^2 \rangle}(x, y) = \frac{\sum_{i=1}^{N} [(V_i - \langle V \rangle)^2 - \sigma_i^2] K((x - X_i)/h_x, (y - Y_i)/h_y)}{\sum_{i=1}^{N} K((x - X_i)/h_x, (y - Y_i)/h_y)} \quad (1)$$

[6] It is perhaps intriguing that our six stars contributing to the cold inner point in Fig. 3*c* are localized—all lie within 3′ of the Sextans center and five occupy a region of diameter 2′. However, Gaussian random samples of 294 stars contain, on average, three mutually exclusive sets of six neighboring stars for which we would measure $\sigma_p \leq 1$ km s$^{-1}$. Including the stars contributing to the cold point in Fig. 3*c*, we detect two such sets in our sample. As they are consistent with what is expected to arise by chance, we conclude that these detections alone do not provide compelling evidence of cold substructure.

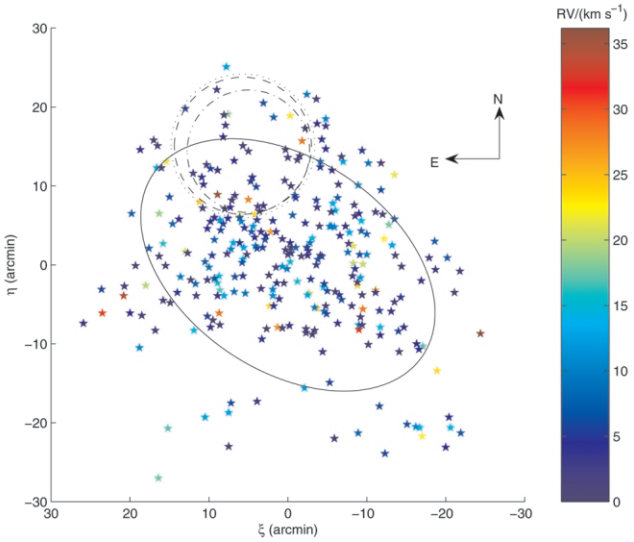


FIG. 2.—Sky map, in standard coordinates, of 303 probable Sextans member stars with velocities measured using MMFS. The color scale indicates the magnitude of each stellar RV relative to the sample mean. The ellipse has geometric mean radius corresponding to $r_{\rm core} = 16'.6 \pm 1'.2$ (Irwin & Hatzidimitriou 1995). The dashed, dotted, and dot-dashed circles respectively enclose the regions from the $N = 294$, $N = 276$, and $N = 303$ samples where the measured RVs are most likely to have been drawn from two distinct Gaussian distributions.

(Nadaraya 1964; Watson 1964), where $\langle V \rangle$ is the sample mean, $K((x - X_i)/h_x, (y - Y_i)/h_y)$ is a smoothing kernel, and $h_x$ and $h_y$ specify spatial smoothing bandwidths. This estimator provides a weighted local average of $\widehat{\langle v^2 \rangle}$ on a grid of $(x, y)$. For simplicity we adopt a bivariate Gaussian kernel with isotropic smoothing: $K((x - X_i)/h_x, (y - Y_i)/h_y) \propto \exp(-\frac{1}{2}[(x - X_i)^2 + (y - Y_i)^2]/h_s^2)$, where $h_s = h_x = h_y$. Since the data points have a nonuniform spatial distribution, we allow the spatial smooth-

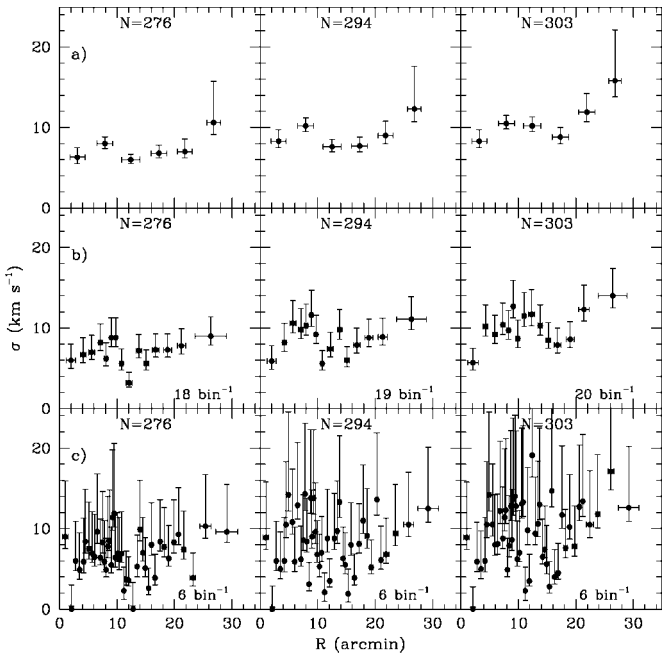


FIG. 3.—Sextans projected velocity dispersion profile measured from the $N = 276$, $N = 294$, and $N = 303$ member samples. Bins in (*a*) have regularly spaced outer boundaries. In (*b*–*c*), bins contain approximately equal numbers of stars. Horizontal error bars indicate the standard deviation of *R*-values.

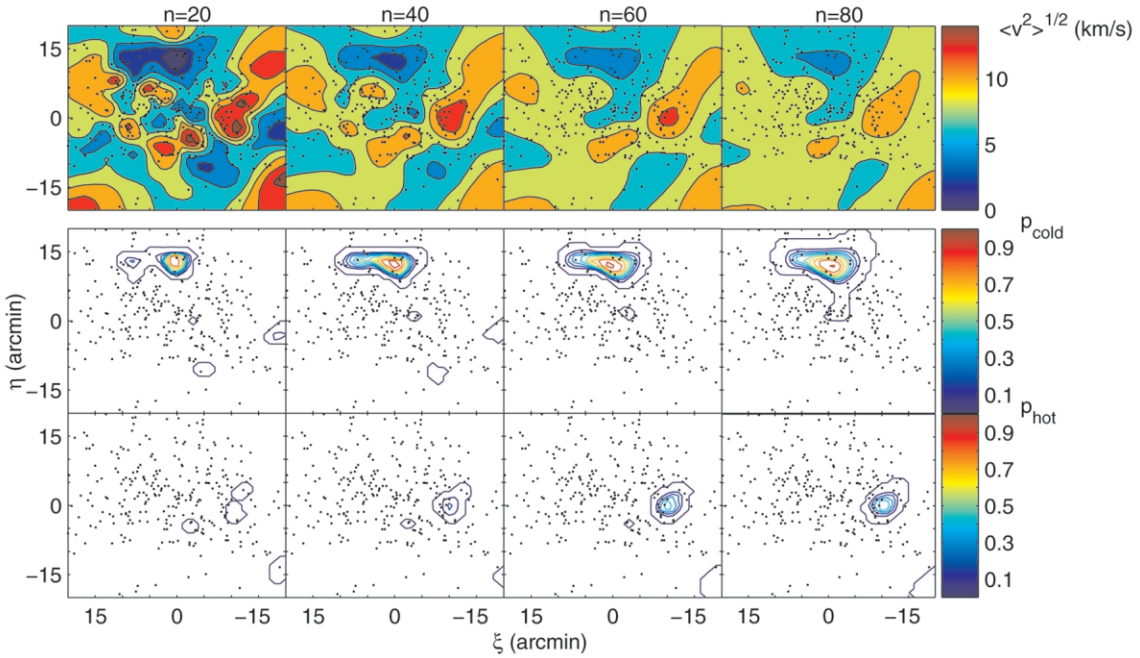


FIG. 4.—*Top*: Contours of the Sextans radial velocity dispersion surface estimate, $\widehat{\langle v^2 \rangle}^{1/2}(x, y)$, obtained by applying eq. (1) to the $N = 294$ member sample. From left to right, panels indicate results from estimations using a nearest neighbor parameter $n$ of 20, 40, 60, and 80. Black dots indicate the positions of member stars used in the estimation. *Middle and bottom*: Contours of statistical significance for regions of apparent cold and hot kinematic substructure; $p_{\rm cold}(x, y)$ is the fraction of artificial data sets for which the simulated surface minimum is greater than the estimate from the Sextans data at $(x, y)$, and $p_{\rm hot}(x, y)$ is the fraction of artificial data sets for which the simulated surface maximum is less than the estimate from the Sextans data at $(x, y)$. Advancing from outermost to innermost, contours enclose regions where $p(x, y) > 0.0, 0.1, 0.2, \ldots, 1.0$.

ing bandwidth, $h_s$, to vary over the grid surface. At every $(x, y)$, $h_s$ takes the minimum value for which there exist $n$ data points located within $3h_s$ of $(x, y)$. The value chosen for $n$ determines the number of neighboring data points that contribute significantly to the kernel.

We use equation (1) to estimate the Sextans RV dispersion surface, $\widehat{\langle v^2 \rangle}_{\rm S}^{1/2}(x, y)$, repeating for neighbor values $n = 10, 20, \ldots, 150$. In all cases we evaluate equation (1) on a square grid with $x$- and $y$-values each spanning the range $\{-20', -19', \ldots, +19', +20'\}$. The top row of panels in Figure 4 maps contours of the Sextans RV dispersion surface resulting from a subset of these estimations with $N = 294$ and $n = 20$, 40, 60, 80.

To assess the significance of apparent surface features, we adopt as a null hypothesis that the measured RVs are drawn everywhere from the same (not necessarily Gaussian) distribution. To simulate the null hypothesis, we generated (for each of the three Sextans samples) 1000 artificial data sets in which the stars have identical positions to those in the Sextans member sample, but in which $(V_i, \sigma_i)$-pairs are drawn randomly, without replacement, directly from the Sextans data. All the observed Sextans RVs are present in each artificial data set, but scrambled with respect to position. This dissociates any existing correlation between position and RV while preserving the global RV distribution.

We apply equation (1) to each artificial data set and record the distributions of artificial surface minima and maxima, $\widehat{\langle v^2 \rangle}_{A,\rm min}$ and $\widehat{\langle v^2 \rangle}_{A,\rm max}$. The significance of a small Sextans surface dispersion at grid point $(x, y)$ is then given by the fraction, $p_{\rm cold}(x, y)$, of artificial surfaces for which $\widehat{\langle v^2 \rangle}_{\rm S}(x, y) < \widehat{\langle v^2 \rangle}_{A,\rm min}$; conversely, the significance of a large Sextans dispersion at $(x, y)$ is given by the fraction, $p_{\rm hot}(x, y)$, of artificial surfaces for which $\widehat{\langle v^2 \rangle}_{\rm S}(x, y) > \widehat{\langle v^2 \rangle}_{A,\rm max}$. The bottom two rows of panels in Figure 4 map contours of $p_{\rm cold}(x, y)$ and $p_{\rm hot}(x, y)$ corresponding to each Sextans RV surface estimation.

For nearly all $n$ and all three cases of membership, the Sextans RV dispersion surface has a minimum value near a point ~15′ north of the Sextans center. For the default $N = 294$ member sample, the significance is $p_{\rm cold} > 0.9$ for estimations in which $30 \le n \le 80$, and it reaches $p_{\rm cold} = 0.965$ for $n = 40$. The same northern region remains the coldest in estimations using the $N = 276$ and $N = 303$ member samples, despite the fact that the former sample removes two stars from within 10′ of the region's center and the latter contributes three high-velocity stars to the region. For $N = 276$, the significance is $p_{\rm cold} > 0.9$ for a wide range of $n$ and reaches $p_{\rm cold} = 0.948$ for $n = 60$.[7] For $N = 303$ the northern feature remains the Sextans surface minimum, but with only $p_{\rm cold} \le 0.671$. The RV distribution at the Sextans *center* does not provide compelling evidence against the null hypothesis. For $N = 276$ and $N = 294$, all surface points inside $R < 5'$ have $p_{\rm cold} < 0.25$; for $N = 303$ the center has $p_{\rm cold} < 0.5$, for all $n$.

We have also employed the parametric test described by Kleyna et al. (2003; K04), which asks whether subregions of the position-RV data are more likely described by a single Gaussian or by a mixture of two distinct Gaussians. This test yields results similar to those from our nonparametric test. For the $N = 294$ sample, a model in which RVs from 80% of the 35 stars centered on a location 15′ north-northeast of the Sextans center (Fig. 2, *dashed circle*) are drawn from a secondary Gaussian with dispersion 2.7 km s$^{-1}$ has likelihood $3.7 \times 10^4$

[7] The $N = 276$ Sextans sample contains a second local minimum, 10′ south of the Sextans center, that is significant with $p_{\rm cold} \sim 0.95$ in estimations using $20 \le n \le 40$. Unlike the northern feature, however, this feature disappears when considering less restrictive membership cases.

times larger than a global Gaussian model. Simulations using artificial data sets indicate this result is sufficient to rule out our null hypothesis with significance $p = 0.968$ (here $p$ indicates the fraction of artificial data sets for which no subregion yields as large a likelihood ratio). For $N = 276$, the same region is kinematically cold (80% of 35 stars drawn from a secondary Gaussian with 2.8 km s$^{-1}$ dispersion) with significance $p = 0.944$. For $N = 303$, the region remains the strongest candidate for cold substructure (60% of 35 stars drawn from a secondary Gaussian with 0 km s$^{-1}$ dispersion), but the significance falls to $p = 0.756$. No aperture overlapping the Sextans center favors a mixed Gaussian model with $p > 0.5$, for any of the three samples and a variety of aperture sizes.

The striking agreement between parametric and nonparametric tests prompts two conclusions: (1) we do not confirm the presence of a kinematically cold Sextans core, and (2) we find stronger evidence ($p \sim 0.95$ for $N = 276$ and $N = 294$) for cold substructure north of center, near the Sextans core radius. The latter result is somewhat sensitive to membership selection—when the most marginal members are allowed into the sample, the significance of the feature drops markedly.

## 3. DISCUSSION

Kleyna et al. have graciously provided us with their RV data for 118 Sextans stars (88 members). Velocity measurements for the 40 stars common to our survey generally agree to within formal uncertainties. For $R < 5'$, the data sets contain two stars in common, with excellent RV agreement. What accounts for the discrepant results between the two studies? Sample size must play a role. K04 propose the existence of a kinematically distinct Sextans core based on the cold RV dispersion of the seven innermost stars in their sample. We find that if we restrict our analyses to similar numbers of stars, we obtain similar evidence. Our RV dispersion profile (Fig. 3*c*) identifies a group of six stars near the Sextans center that have $\sigma_p = 0.0^{+3.3}_{+0.4}$ km s$^{-1}$. If we apply the Gaussian mixture test to the five of these stars clustered nearest a point 3′ north of the Sextans center, a scenario in which four are drawn from a secondary Gaussian with 0 km s$^{-1}$ dispersion is 115 times more likely than the alternative in which all five are drawn from the main Sextans distribution (for comparison, K04 calculate a likelihood ratio of 195 for their cold inner sample). At the location of these five stars, the squared RV dispersion estimated using equation (1) with $n = 5$ is negative, indicating that the measurement uncertainties dominate the scatter among the local velocities. However, for our data neither test result is significant at more than the $p = 0.5$ level.

The substructure candidate we detect lies near the Sextans core radius. If we assume that 80% (the fraction indicated by the Gaussian mixture test) of the stars in the 15′ spanned by this feature belong to a distinct "cluster" of stars and adopt a surface brightness over this region that is constant and equal to one-half Sextans's central surface brightness, we estimate a "cluster" luminosity of $3 \times 10^4\ L_\odot$. This is similar to the luminosity Kleyna et al. (2003) ascribe to the cold clump in UMi but an order of magnitude smaller than the luminosity K04 estimate for a nominal core cluster in Sextans. The timescale for the orbital decay of our "cluster" due to dynamical friction would therefore be an order of magnitude larger than the 0.7–1.5 Gyr that K04 calculate for a core cluster (assuming the same cluster $M/L$ and Sextans halo parameters). This would remove the immediate difficulty in explaining why, if the substructure we detect is associated with a bound cluster, it has not spiraled to the Sextans center. If such a cluster exists, it should be detectable with deep imaging.

Goerdt et al. (2006; see also Sánchez-Salcedo et al. 2006) provide an explanation for the presence of substructure near the core radius of a dSph. They simulate the evolution of globular cluster orbits in the Fornax dSph for both cored and cusped inner dark matter halos. For a cusped halo, dynamical friction drags clusters to the Fornax center on timescales less than 5 Gyr. For a cored halo, the infalling clusters "stall" indefinitely near the dSph core radius, a consequence of what Goerdt et al. interpret as a type of orbital resonance. Thus the presence of five globular clusters near Fornax's core radius strongly favors a cored dark matter halo model. In this context it is intriguing that Ursa Minor and perhaps Sextans also show signs of kinematically cold substructure near their core radii.

We are grateful to Steve Shectman, Rebecca Bernstein, Steve Gunnels, Patrick Kuschack, and Alex Athey for assistance in developing MMFS, and to the staff at Las Campanas Observatory for support. We thank the anonymous referee for helpful comments. This work was supported by NSF grants AST 05-07453, 02-06081, 00-98518, 02-05790, and 05-07511.

## REFERENCES

Beers, T. C., Flynn, K., & Gebhardt, K. 1990, AJ, 100, 32
Bernstein, R., Shectman, S. A., Gunnels, S. M., Mochnacki, S., & Athey, A. E. 2003, Proc. SPIE, 4841, 1694
Coleman, M., Da Costa, G. S., Bland-Hawthorn, J., Martínez-Delgado, D., Freeman, K. C., & Malin, D. 2004, AJ, 127, 832
Coleman, M. G., Da Costa, G. S., Bland-Hawthorn, J., & Freeman, K. C. 2005, AJ, 129, 1443
Goerdt, T., Moore, B., Read, J. I., Stadel, J., & Zemp, M. 2006, MNRAS, in press (astro-ph/0601404)
Irwin, M., & Hatzidimitriou, D. 1995, MNRAS, 277, 1354
Kleyna, J. T., Wilkinson, M. I., Evans, N. W., & Gilmore, G. 2004, MNRAS, 354, L66 (K04)
Kleyna, J. T., Wilkinson, M. I., Gilmore, G., & Evans, N. W. 2003, ApJ, 588, L21 (erratum 589, L59)
Mateo, M. 1998, ARA&A, 36, 435
Muñoz, R. R., et al. 2005, ApJ, 631, L137
Nadaraya, E. A. 1964, Theor. Prob. Appl., 9, 141
Navarro, J. F., Frenk, C. S., & White, S. D. M. 1997, ApJ, 490, 493
Olszewski, E. W., & Aaronson, M. 1985, AJ, 90, 2221
Olszewski, E. W., Mateo, M., Harris, J., Walker, M. G., Coleman, M. G., & Da Costa, G. S. 2006, AJ, 131, 912
Robin, A. C., Reylè, C., Derrière, S., & Picaud, S. 2003, A&A, 409, 523 (erratum 416, 157 [2004])
Sánchez-Salcedo, F. J., Reyes-Iturbide, J., & Hernandez, X. 2006, MNRAS, submitted (astro-ph/0601490)
Tolstoy, E., et al. 2004, ApJ, 617, L119
Walker, M. G., Mateo, M., Olszewski, E. W., Bernstein, R., Wang, X., & Woodroofe, M. 2006, AJ, 131, 2114
Watson, G. S. 1964, Sankhyā–Indian J. Stat., 26, 359
Wilkinson, M. I., Kleyna, J. T., Evans, N. W., Gilmore, G. F., Grebel, E. K., Koch, A., Read, J., & Young, R. 2005, in IAU Colloq. 198, Near-Field Cosmology with Dwarf Elliptical Galaxies, ed. H. Jerjen & B. Binggeli (Cambridge: Cambridge Univ. Press), 240
Wilkinson, M. I., Kleyna, J. T., Evans, N. W., Gilmore, G. F., Irwin, M. J., & Grebel, E. K. 2004, ApJ, 611, L21